2018 18th International Conference on Control, Automation and Systems (ICCAS 2018)
Oct. 17~20, 2018; YongPyong Resort, PyeongChang, GangWon, Korea

Development of Simulator for Autonomous Underwater Vehicles utilizing Underwater Acoustic and Optical Sensing Emulators

Jason Kim, Minsung Sung and Son-Cheol Yu*

Department of Creative IT Engineering
Pohang University of Science and Technology (POSTECH)
Pohang, 37673, Gyeongbuk, South Korea
E-mail: {js21kim, ms.sung, sncyu}@postech.ac.kr

Abstract: This paper addresses an autonomous underwater vehicle (AUV) simulator with underwater image sonar and optical vision emulation. Recently, various underwater missions have been automated through the great improvement in underwater image sonar and optical vision technology along with utilization of artificial intelligence. Development of the simulator that emulates underwater image sonar and optical vision can support intelligent underwater missions by visualizing and simulating virtual scenarios and reproducing real missions. In order to benefit from existing software, the presented simulator is based on ROS (Robot Operating System) environment integrated with our image sonar and optical vision emulators. When an underwater virtual scenario of terrain, target objects, and AUVs with sensors is plotted using standard 3-D modeling programs, the simulator configures the scenario and displays sonar and optical images. The ultrasound and light beams are modeled as a set of rays each, and the image sonar and optical vision are modeled as objects detecting collisions between the rays and target objects at certain positions and orientations. The sonar images generated by the simulator are compared with real images to confirm the validity of the models.

Keywords: underwater simulation, autonomous underwater vehicle, sonar image, optical vision

1. INTRODUCTION

Applications and algorithms for AUVs have been developed for the purpose of deep sea exploration and observation. Various optical vision based researches, such as underwater object recognition and simultaneous localization and mapping (SLAM), have been proposed. Underwater optical vision provides high resolution images with color data in clean and shallow water. However, measuring conditions, such as turbidity of water, intensity of light, and shadows, often greatly restrict the visibility of optical vision. In contrast to optical vision, image sonar is reliable to those underwater conditions. Image sonar can be a good alternative to optical vision, or both sensors can be used together. As display mechanism of image sonar is different from that of optical vision, sonar images are dissimilar to optical images and the vision based algorithms cannot be applied to sonar images. Sonar image based algorithms, such as seabed mosaicking and mapping [1] and 3-D reconstruction [2], are being actively developed.

Experiments with underwater vehicles in open seas or water tanks are costly, risky, and time consuming. It is desirable to develop virtual underwater simulators to test the applications and algorithms before they are deployed on real missions. Several virtual underwater simulators have been developed to serve their own goals. Open source simulators, UWSim and UUV Simulator, show visually realistic 3D geometry with hydrodynamic models [3, 4]. Some simulators are oriented to sonar or optical image simulation without physics and dynamics models [5-7]. To emulate highly intelligent and sophisticated tasks, such as automated object recognition, 3-D reconstruction, and SLAM, we propose a virtual underwater simulator containing dynamics models and sensor models. The presented simulator is developed based on Robot Operating System (ROS) interface to be easily integrated with existing and future ROS plug-ins.

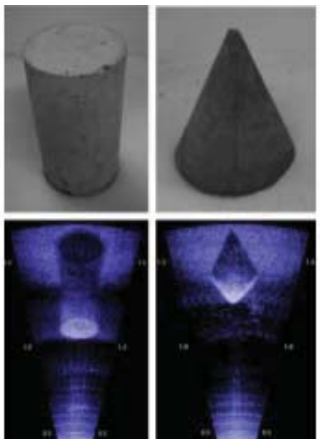

Fig. 1. Sonar and optical images of concrete cylinder and cone

In the remainder of this paper, we briefly describe the image sonar, optical vision, and dynamic models, present simulation results based on the models, and compare them with experimental results.

2. SIMULATOR MODELING

The display mechanism and principle of image sonar is well described in [5] and [6]. While optical vision detects light that is projected from light source and reflected from surfaces of objects, image sonar projects ultrasound beams in the forward direction and detects those that are reflected. Based on the time interval between sending and receiving the ultrasound beams, the image sonar calculates the distance that the ultrasound has traveled. Early returned ultrasound beams form the lower part of the sonar image, and the color becomes brighter in proportion to their intensity. Fig. 1 illustrates

the sonar and optical images that were taken from a same angle and altitude.

2.1 Object

Most standard 3-D modeling software programs use multiple triangular polygons to form surfaces of 3-D objects. The presented simulator reads and stores the 3-D objects in the polygon unit with other data, such as color, acoustic impedance, and absorption ratio of ultrasound and light. The normal vector $\vec{N}$ of a polygon is expressed as

$$\vec{N} = (\overrightarrow{p_2} - \overrightarrow{p_1}) \times (\overrightarrow{p_3} - \overrightarrow{p_1}) \quad (1)$$

where $\overrightarrow{p_1}$, $\overrightarrow{p_2}$, and $\overrightarrow{p_3}$ are the position vectors of the polygon.

2.2 Image Sonar

The image sonar projects ultrasound beams in forward direction within its field of view in azimuth angle θ, elevation angle ϕ, minimum range r_{min}, and maximum range r_{max} as illustrated in Fig. 2. In this paper, we simulate a DIDSON sensor (1.1/1.8 MHz) as the image sonar; θ and ϕ angles range from [-14.5, 14.5] and [-7.0, 7.0] degrees, respectively; r_{min} and r_{max} are set to 0.83 m and 5.83 m, respectively. In our model, the ultrasound beams are considered as a set of rays. There are 96 rays in θ direction and 1,000 rays in the ϕ direction. Therefore, total 96×1000 rays are projected. The reflection of the ultrasound beam from surfaces of target objects is modeled as an intersection between the rays and polygons. If the distance between the acoustic camera and an intersection point is within the range of $[r_{min}, r_{max}]$, this distance can be used to draw the sonar image. In the case where a ray intersects with multiple polygons within the range, only the smallest distance will be used. This is because the ray is reflected and attenuated after the first collision.

The intersection point can be found as follows. We obtain a line equation for a ray and a plane equation for a polygon.

$$\vec{p} = t\vec{v} \quad (2)$$

$$\vec{N} \cdot (\vec{p} - \overrightarrow{p_1}) = 0 \quad (3)$$

where $\vec{p}$ is the intersection point vector, $\vec{v}$ is the normalized direction vector of the ray, and t is a constant. Solving the equations for $\vec{p}$ yields,

$$\vec{p} = \frac{\vec{N} \cdot \overrightarrow{p_1}}{\vec{N} \cdot \vec{v}} \vec{v} \quad (4)$$

Finally, if the three vectors

$$\begin{aligned} &(\overrightarrow{p_2} - \overrightarrow{p_1}) \times (\vec{p} - \overrightarrow{p_1}) \\ &(\overrightarrow{p_3} - \overrightarrow{p_2}) \times (\vec{p} - \overrightarrow{p_2}) \\ &(\overrightarrow{p_1} - \overrightarrow{p_3}) \times (\vec{p} - \overrightarrow{p_3}) \end{aligned} \quad (5)$$

and the normal vector of the plane have the same direction, it is confirmed that the head of $\vec{p}$ lies not only on the plane but inside the polygon.

The modeling of acoustic intensity of the returned beam based on the Lambert's cosine law and acoustic impedance are studied in [6] and [7]. The intensity decreases by the square of the traveled distance R:

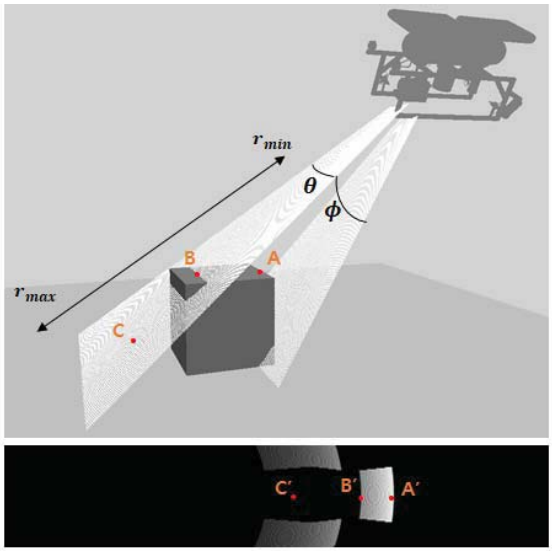

Fig. 2. Image sonar projection model and display mechanism. 3-D points, A, B, and C, are mapped into A′, B′, and C′, respectively in the sonar image.

$$I_I = k\frac{I_0}{R^2} \quad (6)$$

where I_I is the intensity at the intersection point located at distance R from the source, I_0 is the reference intensity at 1 m away from the source, and k is the unit conversion constant. After the reflection, the reflected acoustic intensity I_R is given by

$$I_R = \frac{Z - Z_0}{Z + Z_0} I_I \cos^2 \alpha \quad (7)$$

where Z and Z_0 are the acoustic impedance of the reflected surface and water, and α is the angle between the intersecting ray and polygon. Finally, the measured acoustic intensity I_M is

$$I_M = k\frac{I_R}{R^2} \quad (8)$$

$$= k^2 \frac{Z - Z_0}{Z + Z_0} \frac{I_0}{R^4} \cos^2 \alpha \quad (9)$$

Among the pixels of the sonar image, the pixel of the largest measured intensity is colored white. The gray-scale colors of other pixels are decided by their measured intensity relative to the largest measured intensity.

2.3 Optical Vision

While our image sonar model detects the distance between the source and the object, and the intensity of the returned ultrasound beam, optical vision model simply finds which object is the most closely located, and records its color. The distance values between the light source and object, and between the object and optical camera can be used to calculate the attenuation of light, but they are currently ignored in the model. The model is based on the z-buffer method [8]. Every polygon of objects is projected onto the optical camera window in the method. Then, every pixel of the window searches every point of polygons that is projected onto that pixel, and stores the color of the closest point.

2.4 Dynamic Model of AUV

One of the most widely used dynamic model of an underwater AUV is

$$M(\dot{v}) + C(v)v + D(v)v + W = F \quad (10)$$

derived from Newton-Euler equation where M is the inertia matrix, $C(v)$ is the Coriolis and centripetal matrix, $D(v)$ is the damping matrix, W is the gravitational and buoyancy matrix, and F is the external force matrix acting on the vehicle [9]. A few assumptions are used to simplify (10).

- AUV moves in a low speed.
- AUV is symmetric about the three planes.
- Roll and pitch movements are automatically controlled by AUV.
- AUV's body frame origin is set to its center of gravity.

The assumptions make non-diagonal elements of the dynamic model matrices much smaller than the diagonal elements, and, therefore, the non-diagonal elements can be negligible. The parameters corresponding to roll and pitch movements are omitted. Coriolis and Centripetal force becomes also negligible. In the proposed simulator, the model of Cyclops, a hovering type AUV, is provided [1]. The simplified hydrodynamic model of Cyclops is

$$\begin{aligned} m_u\dot{u} &= -k_u u - k_{u|u|}u|u| + F_u \\ m_v\dot{v} &= -k_v v - k_{v|v|}v|v| + F_v \\ m_w\dot{w} &= -k_w w - k_{w|w|}w|w| + F_w + W_w \end{aligned} \quad (11)$$

where the linear velocities of Cyclops in surge, sway, and heave directions are expressed as u, v, and w; m_u, m_v, and m_w are the summations of masses (weight of Cyclops and added mass terms) in u, v, and w directions; k_u, k_v, k_w, $k_{u|u|}$, $k_{v|v|}$, and $k_{w|w|}$ are the linear and quadratic damping coefficients; F_u, F_v, and F_w are the external forces from thrusters and ocean currents; and W_w is the buoyancy force in w direction. The parameter values obtained from indoor experiments are listed in Table 1 [10].

Table 1. The hydrodynamic parameter values of Cyclops

Parameter	Definition	Value
m	Weight of Cyclops in air	219.8 kg
m_u	Mass in surge	391.5 kg
m_v	Mass in sway	639.6 kg
m_w	Mass in heave	639.6 kg
k_u	Linear damping coefficient in surge	16
k_v	Linear damping coefficient in sway	131.8
k_w	Linear damping coefficient in heave	65.6
$k_{u\|u\|}$	Quadratic damping coefficient in surge	229.4
$k_{v\|v\|}$	Quadratic damping coefficient in sway	328.3
$k_{w\|w\|}$	Quadratic damping coefficient in heave	296.8
W_w	Buoyancy force in heave	-2.5 N

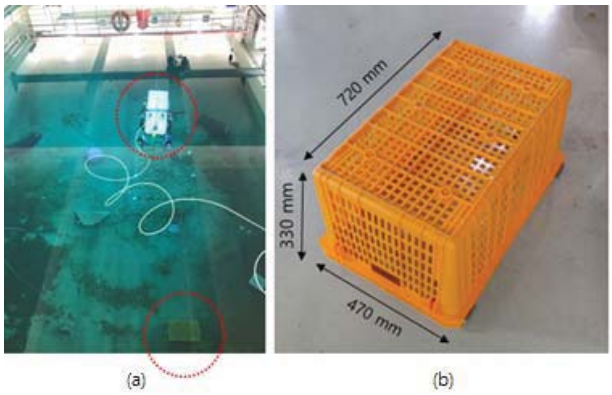

Fig. 3. Experiment environment (a) and the plastic basket used in the experiment (b)

3. Experiments

We performed an experiment to verify the models of the simulator. The experiment was carried out in a water tank. The image sonar was installed at the bottom of the AUV, Cyclops, facing forward and tilted 45 degrees downward. The AUV moved forward 1.5 m above bottom of the water tank, and the image sonar took images of a plastic basket at three different positions. Fig. 3 shows plastic basket used in the experiment and the experimental environment. The same environment was configured in the simulation. The plastic basket was replaced by a cuboid of the same size. An optical vision was installed at the same pose of the image sonar. The acoustic impedance values of water, plastic basket, and concrete floor were set to 1.5×10^6, 3.5×10^6, and 8.0×10^6, respectively.

4. Results

Fig. 4 shows the simulated environment, and real and simulated sonar and optical images. While the image sonar attached at AUV moves forward, only front surface of the object is seen at position A, both front and upper surfaces are seen at position B, and only upper surface is seen at position C. The simulated sonar images exhibit certain characteristics of real images well, such as shape, size, and acoustic intensity along with the distance and slope of the object. However, there are also some differences. First, the real sonar images contain severe noise compared to the simulated images. Second, the colors of shadow regions of the object are not the same; they are black in the simulated images but gray in real images. This is due to the difference between the plastic basket and the solid cuboid. The plastic basket has holes, and some ultrasound beams are not blocked by its front and upper surfaces, and some are reflected. Third, there are circular patterns in the simulated images. These patterns are generated because of poor resolution of ϕ angle. The ϕ angle is divided by 1,000 in our image sonar model. Because 1,000 is not big enough for high resolution, some parts of the target object are failed to be detected and they are shown as black pixels in the simulated images. The accumulated black pixels happen to form the circular patterns in the images. The tighter

angle division can remove the patterns, but the simulation needs more computation power.

5. Conclusion

In this paper, we proposed an underwater virtual simulator with image sonar, optical vision, and dynamics models. The core concepts of the models are the use of polygons for object representation and rays for ultrasound and light beams. On the basis of the model, an image sonar model and optical vision model were developed. We verified the image sonar model by comparing the real and simulated sonar images. The comparison showed good agreement in the shape and color with some differences. To generate more realistic simulated images, uneven backscattering of the ultrasound beams, ocean currents, and errors of AUV movements will be implemented in the future study.

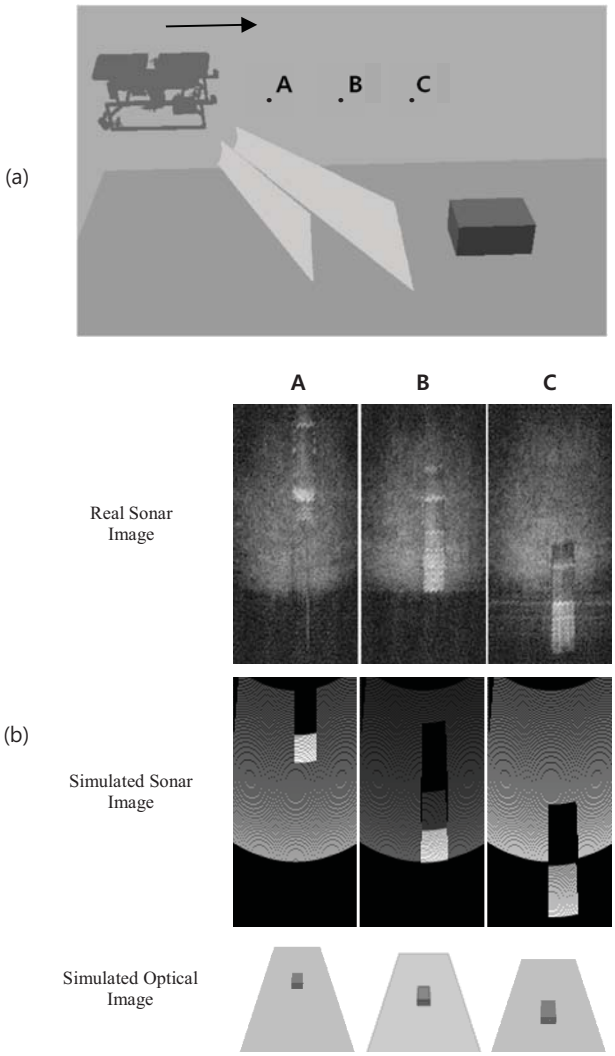

Fig. 4. The sonar and optical images taken at positions A, B, and C of (a) are shown in (b).

ACKNOWLEDGMENT

This research was supported by the MSIT(Ministry of Science and ICT), Korea, under the "ICT Consilience Creative program" (IITP-2018-2011-1-00783) supervised by the IITP(Institute for Information & communications Technology Promotion). This research was a part of the project titled 'Gyeongbuk Sea Grant', funded by the Ministry of Oceans and Fisheries, Korea. This work was supported by the National Research Foundation of Korea(NRF) grant funded by the Korea government(MSIT) (No. 2017R1A5A1014883).

REFERENCES

[1] J. Pyo, H. Cho, H. Joe, T. Ura and S. Yu, "Development of hovering type AUV "Cyclops" and its performance evaluation using image mosaicking", *Ocean Engineering*, 2015, pp. 517-530.

[2] Cho, B. Kim and S. Yu, "AUV-based underwater 3-D point cloud generation using acoustic lens-based multibeam sonar," *Journal of Oceanic Engineering*, 2017, pp. 1-17.

[3] M. Prats, J. Pérez, J. J. Fernández and P. J. Sanz, "An open source tool for simulation and supervision of underwater intervention missions," *2012 IEEE/RSJ International Conference on Intelligent Robots and Systems*, Vilamoura, 2012, pp. 2577-2582.

[4] M. M. M. Manhães, S. A. Scherer, M. Voss, L. R. Douat and T. Rauschenbach, "UUV Simulator: A Gazebo-based package for underwater intervention and multi-robot simulation," *OCEANS 2016 MTS/IEEE Monterey*, Monterey, CA, 2016, pp. 1-8.

[5] J. Gu, H. Joe and S. Yu, "Development of image sonar simulator for underwater object recognition," *2013 OCEANS - San Diego*, San Diego, CA, 2013, pp. 1-6.

[6] E. Catmull, "A subdivision algorithm for computer display of curved surfaces", PhD dissertation, 1974.

[7] S. Kwak, Y. Ji, A. Yamashita and H. Asama, "Development of acoustic camera-imaging simulator based on novel model," *2015 IEEE 15th International Conference on Environment and Electrical Engineering (EEEIC)*, Rome, 2015, pp. 1719-1724.

[8] M. D. Aykin and S. Negahdaripour, "Forward-look 2-D sonar image formation and 3-D reconstruction," *2013 OCEANS - San Diego*, San Diego, CA, 2013, pp. 1-10.

[9] J.H.A.M. Vervoort, "Modeling and control of an unmanned underwater vehicle", 2009.

[10] H. Joe, M. Kim and S. Yu, "Second-order sliding-mode controller for autonomous underwater vehicle in the presence of unknown disturbances", *Nonlinear Dynamics*, 2014, pp. 183-196.